π-Stacking Behavior of Selected Nitrogen-Containing PAHs

Fabien Tran,[†] Bassam Alameddine,[‡] Titus A. Jenny,[‡] and Tomasz A. Wesolowski*[,†]

Department of Physical Chemistry, University of Geneva, 30, quai Ernest-Ansermet, CH-1211 Geneva 4, Switzerland, and Department of Chemistry, University of Fribourg, 9, chemin du Musée, CH-1700 Fribourg, Switzerland

Received: March 23, 2004; In Final Form: July 1, 2004

The packing preferences of dimers formed by nitrogen-containing planar polycyclic aromatic hydrocarbons ($(C_{30}H_{15}N)_2$ and $(C_{36}H_{15}N)_2$) were studied by means of theoretical calculations. Potential energy curves corresponding to various relative motions of the monomers (vertical displacement, rotating, slipping, and combinations of them) were derived. It was found that the monomers in such π-stacked dimers are rather strongly held together (the interaction energy is about −9 kcal/mol) in an off-centered arrangement. It emerges as a general picture that the aligned structures are less stable than the ones where the nitrogen atoms, as the centers of the considered monomers, are not on top of each other but offset by 1.8−2.7 Å. Displacing the centers further results in a rapid reduction of the interaction energy. Within these relatively large relative motions (up to about 3 Å) of the monomers, however, no significant loss of stability of the dimers is noted. In the case of $C_{30}H_{15}N$, changing the orientation of the enantiotopic faces in the dimer formation leads to two nonequivalent minimum energy structures of similar energies but notably different geometries. The most stable structure of both dimers studied resembles that of two adjacent layers of graphite. We conclude, therefore, that the studied molecules could be considered as good building block candidates for the fabrication of columnar organic conductors.

Introduction

π-Stacking, a qualitative conceptual argument frequently used in the discussion of directed intermolecular colligative forces, is poorly quantified by experimental data, and, so far, conventional methods of ab initio theoretical chemistry are not applicable for practical modeling of large π-stacked complexes.[1,2]

Although there is a general consensus concerning the importance of this interaction in almost any field of chemistry, not much is known with respect to its sensitivity to geometrical parameters such as interplanar distance, centroïd dislocation, and torsional angle along the stacking axis. Of minor importance in the case of interaction between small π-systems, for example, the interaction of double bonds with benzene derivatives, these parameters become crucial when considering the stacking of extended polynuclear aromatic systems (PAH) such as hexabenzocoronene (HBC) and its substituted derivatives, an experimentally well-studied class of compounds.[3] Interestingly, this compound shows two distinct stacking patterns depending on the environment: a slipped interaction, resembling the structure of graphite, is found in the crystalline state[4] and produces a similar herringbone pattern as in most crystals of unsubstituted aromatic compounds. Ultrathin layers (up to about eight molecules in thickness) on Cu(111) or Au(111) surfaces, however, arrange in aligned stacks of molecules which show little disorder.[5] Previous calculations (using simple semiempirical method) on trimers and tetramers of coronene,[6] however, indicate stacked-displaced structures as the most stable intermolecular interaction in which the vertical $\pi-\pi$ overlap nearly vanishes, a structure which is neither found in the solid state nor parallels the experimental findings in ultrathin layers of HBC on solid supports.

Nothing is known, however, on the influence of heteroatoms in such systems as exemplified by the benzannelated cyclazine **1** ($C_{36}H_{15}N$). This hitherto unknown molecule could be an interesting candidate for a directional organic conductor if arranged in an extended columnar array, because the presence of a nitrogen atom is expected to lower the oxidation potential of the system considerably. This would render the molecule a nearly perfect hole conductor within the stack.

As the less symmetrical cyclazine **2** ($C_{30}H_{15}N$) was selected as a synthetically easier target instead, the question arose as to what extent the $\pi-\pi$ stacking properties would be influenced by the omission of six peripheral sp^2 carbon atoms.

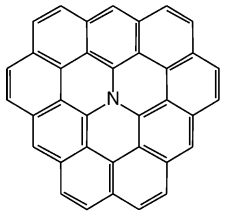

1

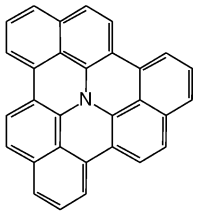

2

Computational Method

To determine the structural preferences of the considered dimers, we analyzed the potential energy curves corresponding to various intermolecular degrees of freedom: vertical distance, rotating, slipping, and their combinations. In the case of cyclazine **2**, we considered also two possible relative orientations

* Corresponding author.
[†] University of Geneva.
[‡] University of Fribourg.

10.1021/jp048713h CCC: $27.50
Published on Web 09/16/2004

of the monomers because the molecule exhibits enantiotopic faces. The conformational analyses were restricted to a parallel arrangement of the molecular planes because any deviation from planarity involves large steric barriers for such extended aromatic systems.

The interaction energies were evaluated using formalism based on the total energy bifunctional $E[\rho_1,\rho_2]$ which offers an alternative to the conventional Kohn−Sham[7] route to approach the ground-state energy in density functional theory[8,9] (DFT). In the bifunctional $E[\rho_1,\rho_2]$, which is a particular case of the multifunctional introduced by Cortona[10] in variational DFT calculations, not only its exchange-correlation part needs to be approximated as an explicit functional of the electron density but also the nonadditive component of the kinetic energy. The bifunctional $E[\rho_1,\rho_2]$ has been used in three types of calculations which differ in the way ρ_1 and ρ_2 are treated such as: (a) ρ_1 and ρ_2 are the electron densities of the isolated monomers as in the model of Gordon and Kim[11] for the evaluation of the interaction energies for weakly bound complexes, (b) ρ_1 and ρ_2 are obtained from the minimization of the bifunctional $E[\rho_1,\rho_2]$,[12] and (c) one of the densities, ρ_1 for instance, is obtained from variational calculations, while ρ_2 is kept frozen, which leads to the orbital-free embedding formalism of Wesolowski and Warshel.[13] In this work, we used the gradient-dependent approximations to the exchange-correlation and nonadditive kinetic-energy components of $E[\rho_1,\rho_2]$. Recently, we demonstrated that the chosen approximations lead to very good interaction energies for a testing set of 25 weakly interacting intermolecular complexes at their equilibrium geometries.[14] They have also been successfully applied in the studies of the potential-energy surface of various other weakly bound complexes including the benzene dimer,[15] and complexes involving benzene,[16] carbazole,[17] and other aromatic carbohydrates.[18] More details concerning the applied method can be found in ref 14. Here, we outline only the specific features relevant to the discussed calculations:

(1) The generalized gradient approximation of Perdew and Wang (PW91)[19] was used for the exchange-correlation energy, and, following the conjointness conjecture of Lee et al.,[20] the reparametrized[21] enhancement factor of the exchange part of the PW91 functional was used to approximate the nonadditive kinetic-energy bifunctional. For weakly overlapping ρ_1 and ρ_2, the applied approximation to the kinetic-energy bifunctional emerged as the most accurate in our rigorous tests.[22,23] Due to the size of the considered systems, we limited the basis set to TZVP.[24] This basis set was demonstrated to approach the basis set limit results in the minimization of the bifunctional $E[\rho_1,\rho_2]$ for the benzene dimer[15] and complexes involving hydrocarbons.[18]

(2) The presented results were obtained using the nonvariational variant of the formalism. The exact expression for the interaction energy ($\Delta E = E[\rho_1,\rho_2] - E[\rho_1^\circ] - E[\rho_2^\circ]$, where ρ_1 and ρ_2 are the electron densities minimizing $E[\rho_1,\rho_2]$ and ρ_1° and ρ_2° are the electron densities of the isolated monomers) was approximated by $\Delta E = E[\rho_1^\circ,\rho_2^\circ] - E[\rho_1^\circ] - E[\rho_2^\circ]$. In the case of the studied complexes, the minimization of the two densities in the complex leads to negligible effects on the interaction energies, resulting in a uniform shift of the potential energy curves. For more discussions on this approximation, see ref 17.

(3) The calculations were performed by means of the modified version of the deMon program[25] into which a formalism performing the variational calculations based on the bifunctional $E[\rho_1,\rho_2]$ was implemented.[12]

The applied computational method is based on first principles. It is, therefore, system-independent. Because it uses only semilocal approximations to the relevant functionals, it cannot describe properly the interactions between nonoverlapping electron densities. However, if the overlap between the electron densities of the interacting molecules is not negligible, as is the case for the systems studied in the present work, the applied method was shown to lead to very accurate interaction energies, typically significantly better than the ones derived using the conventional Kohn−Sham formalism.[14] Moreover, the functional used to calculate the Coulomb interactions, which were shown by Hunter and Sanders[26] to determine the structure of stacked $\pi-\pi$ complexes, is evaluated exactly for a given pair of electron densities in the applied formalism. For these reasons, we have chosen the bifunctional method for this study aimed at predicting the structural preferences of dimers bound by noncovalent interactions.

Results

Several types of intermediate geometries are discussed throughout this work. For each dimer, we started with the structure in which the corresponding atoms are localized exactly on top of each other (arrangement of the highest symmetry). The conformational energy search was performed by analyzing the potential energy curves corresponding to the variations of the following intermolecular degrees of freedom: interplanar distance z, angle ϕ of rotation about the C_3 axis of one of the monomers (see Figure 1a), and the degrees of freedom associated with slipping one monomer on the other: magnitude r and direction α (see Figure 1b). Because the two faces of cyclazine **2** are enantiotopic and hence not equivalent, two types of dimers were considered: one with the same orientation of the faces of the monomers, that is, both *si*-faces up (=achiral *meso*-dimer), and the other with the opposite orientation, that is, both *si*-faces at the inside (=chiral dimer). It is worthwhile to notice that, in the case of the opposite orientation of the faces of the cyclazine **2** dimer, localization for each atom exactly on top of their corresponding partners is not possible.

$(C_{30}H_{15}N)_2$: *meso*-Dimer. In the highest symmetry arrangement of this dimer, the interaction energy varies rapidly with the interplanar distance and reaches the minimum of $\Delta E = -5$ kcal/mol at $z = 3.45$ Å. Rotating one monomer about its C_3 axis increases the interaction energy further (see Figure 2a), which leads to a new minimum ($\Delta E = -7.0$ kcal/mol) at $\phi = 30°$. Continued rotation reduces the interaction energy very slightly, reaching -6.8 kcal/mol at $\phi = 60°$. Due to the symmetry of the dimer, the potential energy curve for $60° < \phi < 120°$ is the mirror image of the one for $0° < \phi < 60°$, which yields a rather flat potential energy curve for $30° < \phi < 90°$. Reoptimizing the interplanar distance for $\phi = 30°$ and $\phi = 60°$ leads to an almost uniform shift of the potential energy curve to $\Delta E = -7.4$ kcal/mol and $\Delta E = -7.1$ kcal/mol, respectively, at $z = 3.3$ Å.

The next step in the conformational analysis consisted of analyzing the energetic effects associated with slipping one monomer with respect to the other. Starting from the ($\phi = 60°$, $z = 3.3$ Å)-structure, one of the monomers was shifted by the distance r. The potential energy curves corresponding to $\alpha = 0°$, 30°, 60°, and 90° are shown in Figure 2b. The deepest minimum $\Delta E = -8.4$ kcal/mol was found for $\alpha = 0°$ at $r = 2.7$ Å. Figure 3a shows this minimum energy structure. Interestingly, but perhaps not surprising, every second atom of one monomer is aligned with an atom of the other monomer, an arrangement as it occurs in graphite. Starting from the ($\phi =$

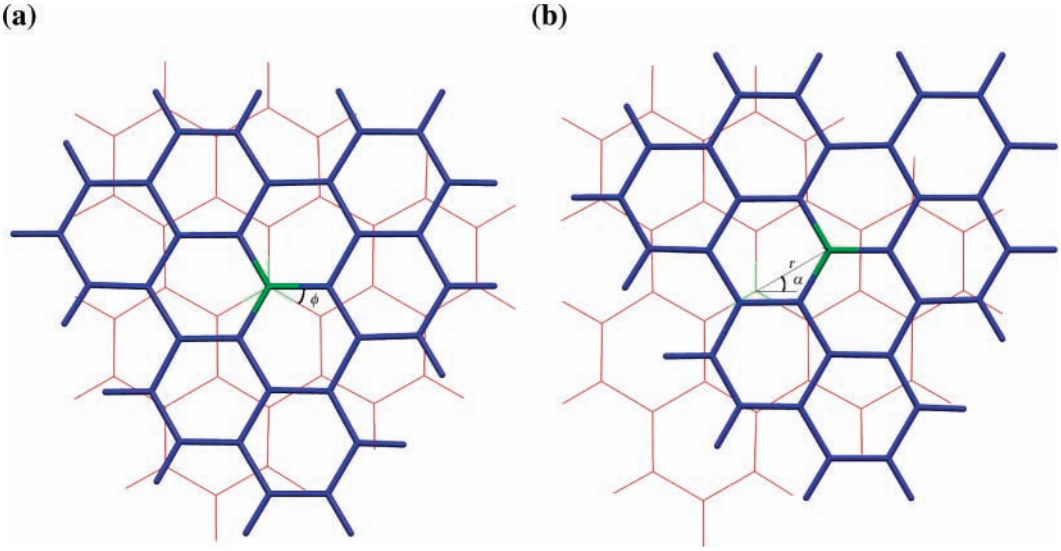

Figure 1. Top view of the $(C_{30}H_{15}N)_2$ dimer showing the intermolecular degrees of freedom considered in this work: the angles ϕ and α, and the distance r. The central nitrogen atom of each monomer is in green, and the remaining atoms (carbon and hydrogen) are in red for one monomer and in blue for the other.

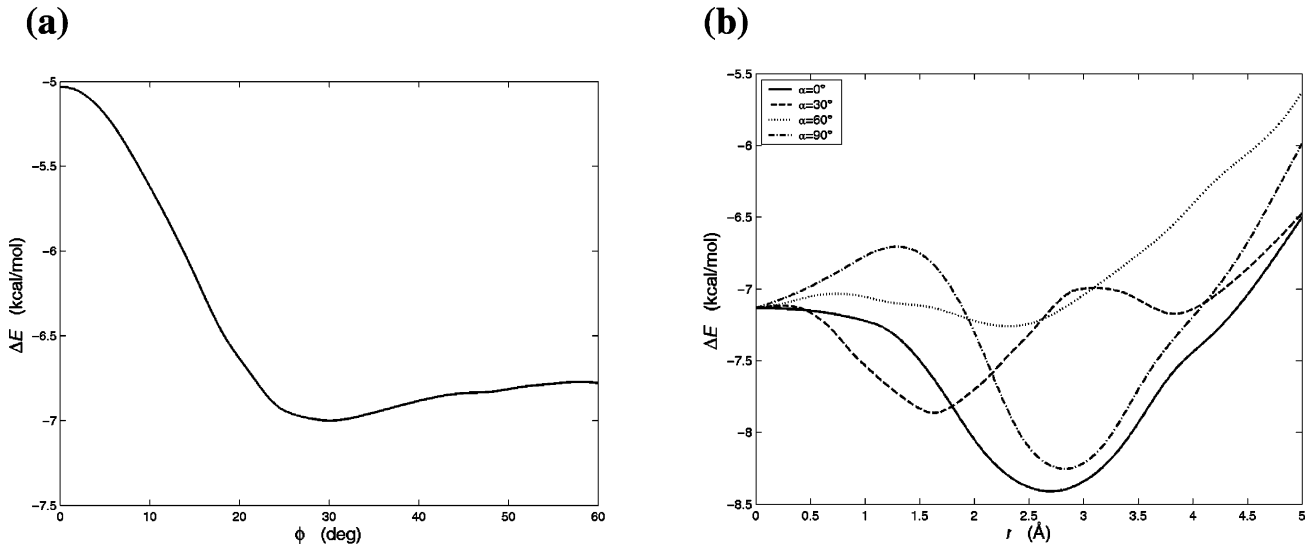

Figure 2. Interaction energy ΔE for the *meso*-dimer $(C_{30}H_{15}N)_2$: (a) ΔE as a function of the angle ϕ, (b) ΔE as a function of the parallel displacement r for $\phi = 60°$ and several directions α. For the description of the angles, see Figure 1.

30°, $z = 3.3$ Å)-structure yields very similar curves not leading to a more stable geometry, however.

$(C_{30}H_{15}N)_2$: Chiral Dimer. In the starting structure (the highest symmetry arrangement), the two nitrogen atoms are again localized exactly on top of each other, but, opposite to the previously discussed case, not every atom of one monomer finds its partner in the other monomer. In this arrangement, the interplanar distance z at minimum energy is similar to the one found for the *meso* case ($\Delta E = -6.8$ kcal/mol at $z = 3.36$ Å). Rotating one monomer about its C_3 axis leads to the potential energy curve shown in Figure 4a. The lowest minimum ($\Delta E = -7.5$ kcal/mol) occurs at this time at $\phi = 20°$ already. Reoptimizing the interplanar distance to $z = 3.29$ Å does not noticeably increase the interaction energy, but, as compared to the *meso* case, the potential energy curve is less smooth and shows two distinct maxima at 48° and 88°.

The potential energy curves corresponding to slipping at α = 0°, 30°, 60°, and 90°, starting from the ($\phi = 20°$, $z = 3.29$ Å)-geometry, are shown in Figure 4b. All four curves show a similar trend: they start at an energy minimum and reach, after a low barrier at 1−1.5 Å, the second energy minimum at 2.5−3.5 Å. For α = 0° and $r = 3.5$ Å (cf. Figure 3b), this minimum is deeper ($\Delta E = -7.8$ kcal/mol) than the previous one.

$(C_{36}H_{15}N)_2$. For this dimer, the potential energy surface was analyzed in the same order as in the previously discussed cases starting from the highest symmetry arrangement for which the energy minimum of $\Delta E = -6.3$ kcal/mol occurs at $z = 3.47$ Å. The potential energy curve corresponding to the rotation about the C_3 axis shown in Figure 5a resembles that of the *meso*-dimer of **2**, but shows a more pronounced angle dependence as compared to the previous case. Between $\phi = 0°$ and $\phi = 120°$, two distinct minima of $\Delta E = -7.7$ kcal/mol and $\Delta E = -7.5$ kcal/mol appear at $\phi = 24°$ and $\phi = 60°$, respectively. The two minima are separated by a small energy barrier at $\phi = 45°$. Reoptimizing the intermolecular distance z leads to a decrease of the energy at −8.0 kcal/mol and −7.8 kcal/mol for $\phi = 24°$ and $\phi = 60°$, respectively, and a slightly shorter interplanar distance amounting to $z = 3.35$ Å at either minimum.

As in the previously discussed cases, the potential energy curves involving slipping of the monomers were calculated starting from the minimum energy geometry ($\phi = 60°$, $z = 3.35$ Å) for the directions α = 0°, 30°, 60°, and 90° as shown in

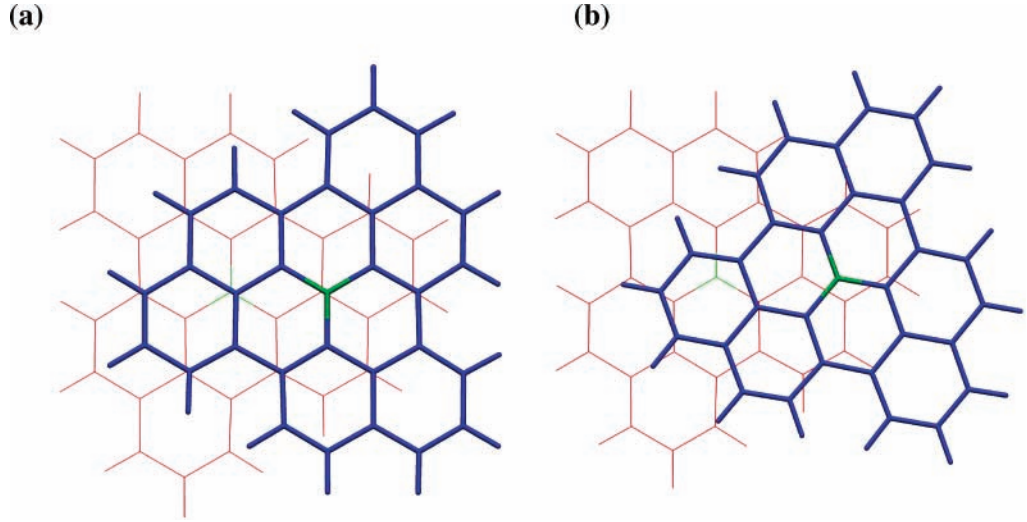

Figure 3. The minimum energy structures of the $(C_{30}H_{15}N)_2$ dimer: (a) the most stable structure for the *meso*-dimer, (b) the most stable structure for the chiral dimer. The color of the atoms follows the same convention as that in Figure 1.

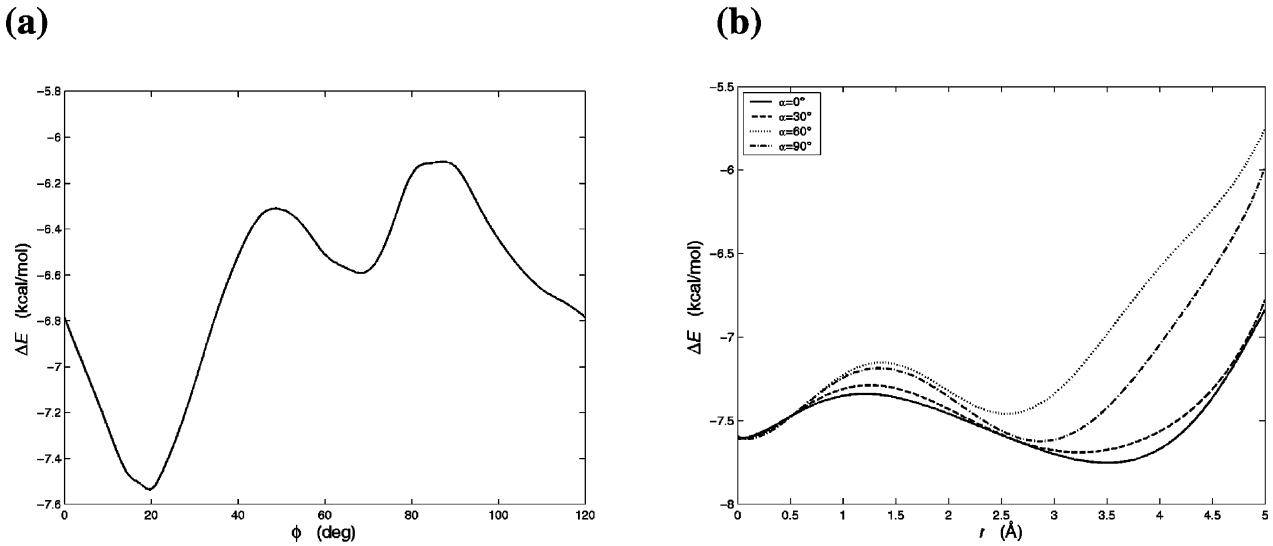

Figure 4. Interaction energy ΔE for the $(C_{30}H_{15}N)_2$ chiral dimer: (a) ΔE as a function of the angle ϕ, (b) ΔE as a function of the parallel displacement r for $\phi = 20°$ and several directions α. For the description of the angles, see Figure 1.

Figure 5b. The deepest minimum ($\Delta E = -9.6$ kcal/mol) was found for $\alpha = 30°$ and $r = 1.8$ Å. Figure 6 shows this minimum energy structure which is very similar to the minimum energy structure of the $C_{30}H_{15}N$ *meso*-dimer (cf. Figure 3a). However, the atoms of one monomer are not localized exactly on top of an atom or a ring center of the other monomer, but are slightly shifted. The three other curves ($\alpha = 0°$, 60°, and 90°) lead to less deep minima occurring at considerably larger slipping distances (r close to 3 Å). Similar analyses of the potential energy curves starting from the geometry of the other minimum found in the previous step ($\phi = 24°$, $z = 3.35$ Å) lead to smaller interaction energies.

Discussion

It is appealing to analyze the energy differences derived from our calculations in terms of the number of carbon−surface contacts. Theoretical and experimental[27−32] studies indicate that a single carbon−surface contact at a favorable structural arrangement can contribute to the interaction energy as much as 3.11 kcal/mol.[27−31] Clearly, our calculated binding energies per contact are much smaller. For instance, there are 26 contacts at the global minimum geometry of $(C_{36}H_{15}N)_2$ (see Figure 6), which yield 0.37 kcal/mol per contact. At this stage, it might be useful to differentiate between two types of contacts: (a) contacts involving only atoms in the interior of the molecule such as the ones occurring in the infinite sheets in graphite, and (b) contacts involving edge atoms of one monomer and interior atoms of the other such as the ones occurring for alkanes adsorbed on graphite surface. On the basis of our results, we conclude that the contacts of the latter type are more important because the minimum energy structures found in this work maximize the number of contacts between the edge atoms of one molecule and the interior atoms of the other at the expense of the contacts formed by two interior atoms. Therefore, the stabilizing effect of the edge atoms (rim effect) emerging from this study can be expected to be the dominating factor determining the structure of complexes such as those analyzed in the present work.

The remarkable structural similarity between the relative arrangement of the two monomers in the minimum geometry of either the *meso*-dimer of $(C_{30}H_{15}N)_2$ or the $(C_{36}H_{15}N)_2$ dimer and the arrangement of two graphite layers indicates that the presence of the nitrogen atom does not influence significantly the stacking interactions. To make a more detailed assessment

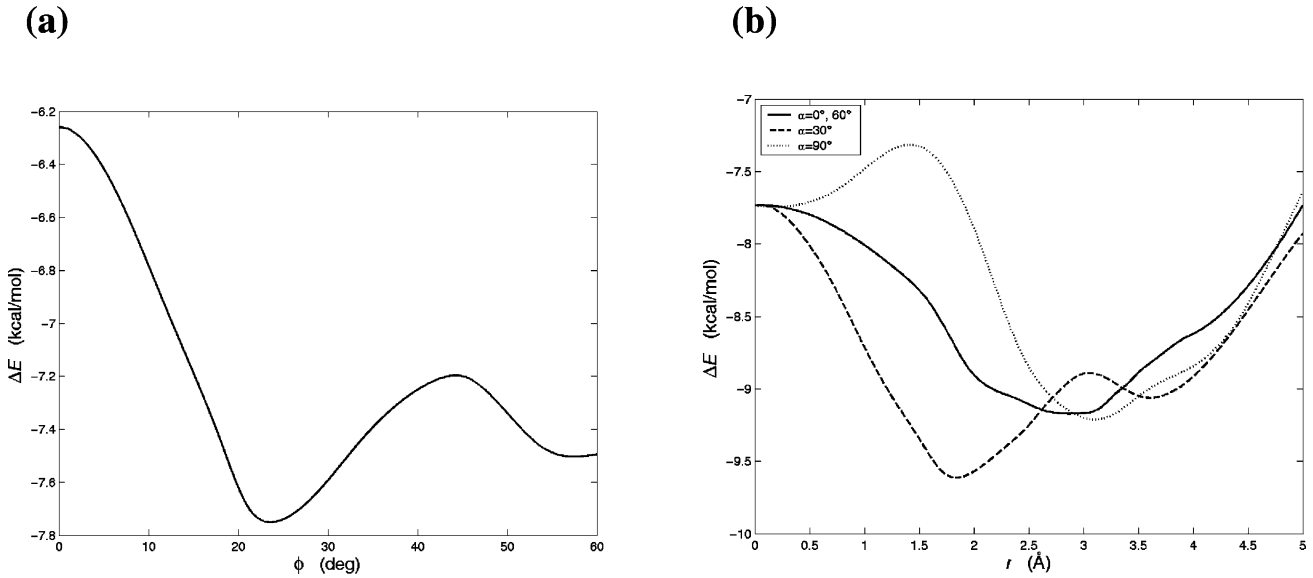

Figure 5. Interaction energy ΔE for the $(C_{36}H_{15}N)_2$ dimer: (a) ΔE as a function of the angle ϕ, (b) ΔE as a function of the parallel displacement r for $\phi = 60°$ and several directions α. For the description of the angles, see Figure 1.

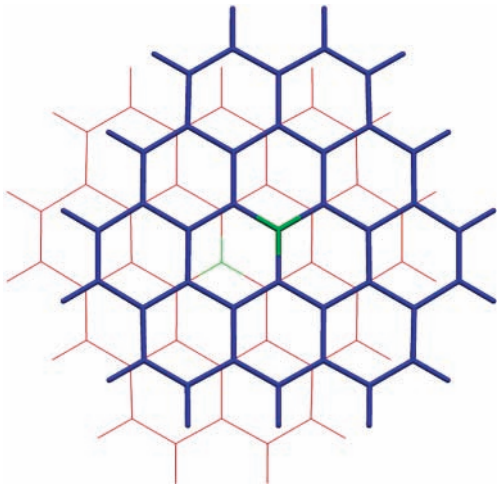

Figure 6. The most stable structure of the $(C_{36}H_{15}N)_2$ dimer. The color of the atoms follows the same convention as that in Figure 1.

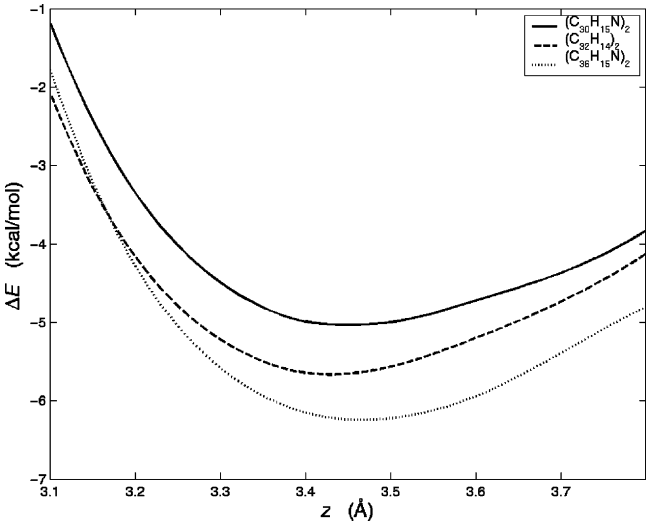

Figure 7. Interaction energy ΔE as a function of the interplanar distance z for $(C_{32}H_{14})_2$, $(C_{30}H_{15}N)_2$, and $(C_{36}H_{15}N)_2$ dimers in the highest symmetry arrangement.

of the effect of the nitrogen atom, the potential energy curve corresponding to the variation of the intermolecular z distance of two perfectly aligned ovalene ($C_{32}H_{14}$) molecules is shown in Figure 7. The ovalene molecule was chosen because of its similarity to the two nitrogen-containing PAHs studied in this work. Indeed, as compared to the nitrogen-free reference ovalene dimer, z increases negligibly due to the presence of the nitrogen atom (by 0.02 and 0.04 Å for $(C_{30}H_{15}N)_2$ and $(C_{36}H_{15}N)_2$, respectively). As far as the interaction energy ΔE is concerned, the potential energy curve of $(C_{32}H_{14})_2$ lies between those of $(C_{30}H_{15}N)_2$ and $(C_{36}H_{15}N)_2$, reflecting thus the fact that the interaction energy correlates with the number of contacts between atoms of different monomers.

Conclusions

The theoretical studies of π-stacking of two selected nitrogen-containing PAHs reveal features of great relevance for their possible role as building blocks of columnar structures.

The minimum geometries of all considered dimers are off-centered. At such an arrangement, the number of possible contacts is reduced as compared to a perfectly aligned stacked dimer. We attribute the fact that the slipped geometry is more stable than the centered one to the difference in stability between the edge−interior and interior−interior contacts (rim effect), which dominates the molecule−molecule interaction and determines the overall geometry of the stacked dimers.

The nonnegligible energy difference (0.6 kcal/mol) between the *meso*- and chiral dimers of $C_{30}H_{15}N$ indicates the surprising possibility of a shape recognition phenomenon, which is expected to yield, experimentally, the more stable configuration, that is, the *meso*-typed stacks of $C_{30}H_{15}N$ exclusively. The origin of this energy difference can be qualitatively explained by a higher number of stabilizing atom−atom contacts in the $C_{30}H_{15}N$ *meso*-dimer (Figure 3a) than in the chiral $C_{30}H_{15}N$ dimer (Figure 3b). This interpretation is supported by the fact that the $(C_{36}H_{15}N)_2$ dimer with a larger number of contacts is more stable than the $C_{30}H_{15}N$ *meso*-dimer ($\Delta E = -9.6$ vs $\Delta E = -8.4$ kcal/mol).

Finally, we notice that the presence of nitrogen in the center of the analyzed monomers does not imply any apparent preferences as the structure of the dimers is concerned.

In summary, N-containing highly extended aromatic systems can be expected to be very good building blocks of π-stacked

complexes, in which the central nitrogen atoms does not disturb the intermolecular interactions significantly. This triggers the way toward the synthesis of such columnar arrays and their use as promising organic hole conductors excelling the all-carbon PAHs.

Acknowledgment. This work is part of projects 200020-100352 and 4047-057525 of the Swiss National Science Foundation.

References and Notes

(1) Hobza, P.; Zahradník, R. *Chem. Rev.* **1988**, *88*, 871−897.
(2) Chalasinski, G.; Szczesniak, M. M. *Chem. Rev.* **2000**, *100*, 4227−4252.
(3) Brown, S. P.; Schnell, I.; Brand, J. D.; Müllen, K.; Spiess, H. W. *J. Mol. Struct.* **2000**, *521*, 179−195.
(4) Kübel, C.; Eckhardt, K.; Enkelmann, V.; Wegner, G.; Müllen, K. *J. Mater. Chem.* **2000**, *10*, 879−886.
(5) Ruffieux, P.; Gröning, O.; Bielmann, M.; Simpson, C.; Müllen, K.; Schlapbach, L.; Gröning, P. *Phys. Rev. B* **2002**, *66*, 073409-1−073409-4.
(6) Rodríguez, J.; Sánchez-Marín, J.; Torrens, F.; Ruette, F. *J. Mol. Struct. (THEOCHEM)* **1992**, *254*, 429−441.
(7) Kohn, W.; Sham, L. J. *Phys. Rev.* **1965**, *140*, A1133−A1138.
(8) Hohenberg, P.; Kohn, W. *Phys. Rev.* **1964**, *136*, B864−B871.
(9) Parr, R. G.; Yang, W. *Density-Functional Theory of Atoms and Molecules*; Oxford University Press: Oxford, 1989.
(10) Cortona, P. *Phys. Rev. B* **1991**, *44*, 8454−8458.
(11) Gordon, R. G.; Kim, Y. S. *J. Chem. Phys.* **1972**, *56*, 3122−3133.
(12) Wesolowski, T. A.; Weber, J. *Chem. Phys. Lett.* **1996**, *248*, 71−76.
(13) Wesolowski, T. A.; Warshel, A. *J. Phys. Chem.* **1993**, *97*, 8050−8053.
(14) Wesolowski, T. A.; Tran, F. *J. Chem. Phys.* **2003**, *118*, 2072−2080.
(15) Tran, F.; Weber, J.; Wesolowski, T. A. *Helv. Chim. Acta* **2001**, *84*, 1489−1503.
(16) Wesolowski, T. A.; Ellinger, Y.; Weber, J. *J. Chem. Phys.* **1998**, *108*, 6078−6083.
(17) Wesolowski, T. A.; Morgantini, P.-Y.; Weber, J. *J. Chem. Phys.* **2002**, *116*, 6411−6421.
(18) Tran, F.; Weber, J.; Wesolowski, T. A.; Cheikh, F.; Ellinger, Y.; Pauzat, F. *J. Phys. Chem. B* **2002**, *106*, 8689−8696.
(19) Perdew, J. P.; Chevary, J. A.; Vosko, S. H.; Jackson, K. A.; Pederson, M. R.; Singh, D. J.; Fiolhais, C. *Phys. Rev. B* **1992**, *46*, 6671−6687; **1993**, *48*, 4978(E).
(20) Lee, H.; Lee, C.; Parr, R. G. *Phys. Rev. A* **1991**, *44*, 768−771.
(21) Lembarki, A.; Chermette, H. *Phys. Rev. A* **1994**, *50*, 5328−5331.
(22) Wesolowski, T. A.; Chermette, H.; Weber, J. *J. Chem. Phys.* **1996**, *105*, 9182−9190.
(23) Wesolowski, T. A. *J. Chem. Phys.* **1997**, *106*, 8516−8526.
(24) Godbout, N.; Salahub, D. R.; Andzelm, J.; Wimmer, E. *Can. J. Chem.* **1992**, *70*, 560−571.
(25) (a) St-Amant, A.; Salahub, D. R. *Chem. Phys. Lett.* **1990**, *169*, 387−392. (b) St-Amant, A. Ph.D. Thesis, University of Montreal, 1992. (c) Casida, M. E.; Daul, C.; Goursot, A.; Koester, A.; Pettersson, L. G. M.; Proynov, E.; St-Amant, A.; Salahub, D. R., principal authors; Chretien, S.; Duarte, H.; Godbout, N.; Guan, J.; Jamorski, C.; Leboeuf, M.; Malkin, V.; Malkina, O.; Nyberg, M.; Pedocchi, L.; Sim, F.; Vela, A., contributing authors. *deMon-KS version 3.5*; deMon Software, 1998.
(26) Hunter, C. A.; Sanders, J. K. M. *J. Am. Chem. Soc.* **1990**, *112*, 5525−5534.
(27) Weber, S. E.; Talapatra, S.; Journet, C.; Zambano, A.; Migone, A. D. *Phys. Rev. B* **2000**, *61*, 13150−13154; **2002**, *66*, 049901(E).
(28) Zhao, X.; Kwon, S.; Vidic, R. D.; Borguet, E.; Johnson, J. K. *J. Chem. Phys.* **2002**, *117*, 7719−7731.
(29) Paserba, K. R.; Gellman, A. J. *J. Chem. Phys.* **2001**, *115*, 6737−6751.
(30) Ugalde, J. M. *J. Phys. Chem. B* **2002**, *106*, 6871−6874.
(31) Lee, N. K.; Park, S.; Kim, S. K. *J. Chem. Phys.* **2002**, *116*, 7902−7909.
(32) Ruoff, R. S.; Hickman, A. P. *J. Phys. Chem.* **1993**, *97*, 2494−2496.